**Accepted manuscript,** https://doi.org/10.1016/j.surfcoat.2019.125107



# Effect of processing and interface on the durability of single and bilayer 7YSZ / Gadolinium Zirconate EB-PVD thermal barrier coatings

Uwe Schulz[a, *], Andrzej Nowotnik[b], Stefan Kunkel[c], Georg Reiter[c]

[a]German Aerospace Center (DLR), Cologne 51147, Germany

[b]Rzeszow University of Technology, 35-959 Rzeszow, Poland

[c]ALD Vacuum Technologies GmbH, 63457 Hanau, Germany

## Abstract

Gadolinium Zirconate (GZO) is known for its low thermal conductivity, high thermal stability and a favorable fast reaction with CMAS deposits that makes such a thermal barrier coating (TBC) more stable and less infiltrated in dusty turbine environments. In the present study, Electron Beam Physical Vapor deposited (EB-PVD) GZO / 7YSZ bilayers were coated on superalloy bars having a NiCoCrAlY bond coat. Two different coaters that were either pilot production / lab scale size suitable for coating development (coater ESPRI) or small scale production / development size (SMART Coater) suitable for both development and production were used. The bilayers were compared to single layers of 7YSZ or GZO, respectively. Beside lifetime investigations of the various TBC systems special emphasis was put on the interface architecture between 7YSZ and GZO. The coatings where the transition between the two layers was done rapidly achieved the longest lifetime of all bilayers, regardless of the EB-PVD coater used. Nearly all GZO top coats showed a longer lifetime than the standard 7YSZ systems in furnace cycling testing at 1100°C.

**Keywords:** Thermal Barrier Coatings; EB-PVD; Gadolinium Zirconate; Bilayer

**Corresponding Author. Tel.: +49 2203 601 2543; Fax: +49 2203 696480.*

*E-mail address: Uwe.Schulz@dlr.de*

## 1. Introduction

Thermal barrier coatings (TBCs) having compositions other than the commonly used yttria-stabilized zirconia (7 to 8 wt% $Y_2O_3$ – $ZrO_2$ including up to around 2 wt% $HfO_2$ as natural impurity - 7YSZ) have attracted much interest over the last decade. Among them, gadolinium zirconate $Gd_2Zr_2O_7$ (GZO) is one of the most prominent examples introduced into aero-engines several years ago. Numerous studies have been published on GZO TBCs manufactured by a variety of techniques such as air plasma spraying, suspension plasma spraying, and electron-beam physical vapor deposition (EB-PVD) [1-8]. The advantages of GZO comprise an improved behavior under deposits such as CMAS or volcanic ash by drastically lowering the infiltration depth and the stiffened layer thickness, a lower thermal conductivity, and improved phase stability. Drawbacks of this material include higher raw material cost, a reduced fracture toughness that leads to a lower erosion resistance and a different cracking behavior, a lower coefficient of thermal expansion, and a possible incompatibility with alumina as main constituent of the thermally grown oxide (TGO) on top of the bond coat [2, 3, 9-12]. Alumina in the TGO and the pyrochlore and/or cubic phase of GZO are not in equilibrium and tend to form $GdAlO_3$ after prolonged high temperature exposure [10, 13]. While on NiCoCrAlY [6] and CoNiCrAlY bond coats [7, 8] such phase formation was observed during high temperature annealing and testing of GZO single EB-PVD layers, no reaction was found on a Hf-doped NiCoCrAlY that consist of alumina and hafnia particles [5].

To overcome the limitations of single GZO layers, bilayer TBCs consisting of a first 7YSZ base layer and a thicker GZO top layer have been introduced. This has been successfully demonstrated for both thermal sprayed coatings [3, 4, 14, 15] and EB-PVD coatings [6-8, 16-18]. Most of those studies revealed a longer lifetime of the bilayers compared to single layer GZO, single layer 7YSZ, or both. In contrast to those findings, in some of our previous studies we could achieve a longer lifetime of single layer GZO coatings if applied properly on a NiCoCrAlY bond coat, albeit of some reactions with the TGO [5, 6, 19]. While phase formation in the top layer, reactions with CMAS or volcanic ash, TGO formation, failure behavior under isothermal, furnace cycle testing (FCT), and temperature gradient conditions have been widely evaluated for 7YSZ/GZO bilayers, the interface architecture between the two layers has not been studied in detail. Therefore, the current study concentrates on the influence of processing conditions and the interface design of the two ceramic layers on microstructure and lifetime of the TBCs. The coatings were manufactured in two different EB-PVD coaters to elaborate the impact of different equipment on the results. The bilayers of 7YSZ/GZO were compared to single layers of both 7YSZ and GZO with special emphasis on lifetime and microstructure.

## 2. Experimental Procedure

Cylindrical rods of the superalloy IN100 with a diameter of 6mm and a length of around 60mm were used as substrates. They were coated with a NiCoCrAlY bond coat of 80-115µm thickness by EB-PVD using a 150kW EB-PVD coater at DLR. The measured composition of the samples was Ni (bal.) - 21 to 22Co – 16 to 20Cr - 12 to 13Al - 0.2 to 0.4Y (wt%). All NiCoCrAlY bond coats were densified by ball peening and subsequently vacuum annealed at 1080°C for 4 hours as commonly done for this bond coat before deposition of ceramic top coat layers.

Two different coaters were used in this study for the application of the TBCs. At DLR the 150kW EB-PVD unit ESPRI equipped with chambers for loading, pre-heating, and deposition was used. Samples were fixed on a planetary rotation sample holder that can hold up to eight samples at a time. ESPRI is equipped with one EB gun with a maximum of 150kW power which is capable of evaporating from two crucibles that are arranged in a pre-defined flexible, but during the run fixed position with regard to the chamber and rotation shaft axis. During the present experiments the two crucibles were exactly aligned in the axis of the shaft that provides sample transfer between the vacuum chambers and the rotation of the samples in the planetary drive. Eight samples were coated in each run with a rotation rate of the individual samples of 12 rpm. To form the bilayer the shaft was moved from the 7YSZ-crucible to the GZO crucible.

At Rzezow University the SMART Coater was used for deposition of the top layers. It also comprises chambers for loading, pre-heating, and deposition. Samples were fixed on a rake comprising three separate position for fixing blades or samples. In each position one holder for one pin or up to six buttons were attached. The three positions are arranged in a manner that the middle position is always arranged centered above the evaporation pool while the other two are slightly off. The SMART Coater is equipped with one EB gun with a maximum 160kW output and which is also capable of evaporating from two crucibles. The two crucibles are arranged perpendicular to the sample rotation axis, but in line with the main telescope sting. The two crucibles can be moved during the run in a direction parallel to the main sting axis while evaporation continues to form the bilayer. Movements for tilting of the samples were not applied in the current experiments.

Figure 1 shows the two coaters used in this study while Figure 2 summarizes schematically the geometric conditions within the deposition chambers during evaporation.

(a)

(b)

Figure 1: EB-PVD coating equipment used in the current study. (a) Coater ESPRI at DLR, and (b) SMART coater at Rzeszow University of Technology.

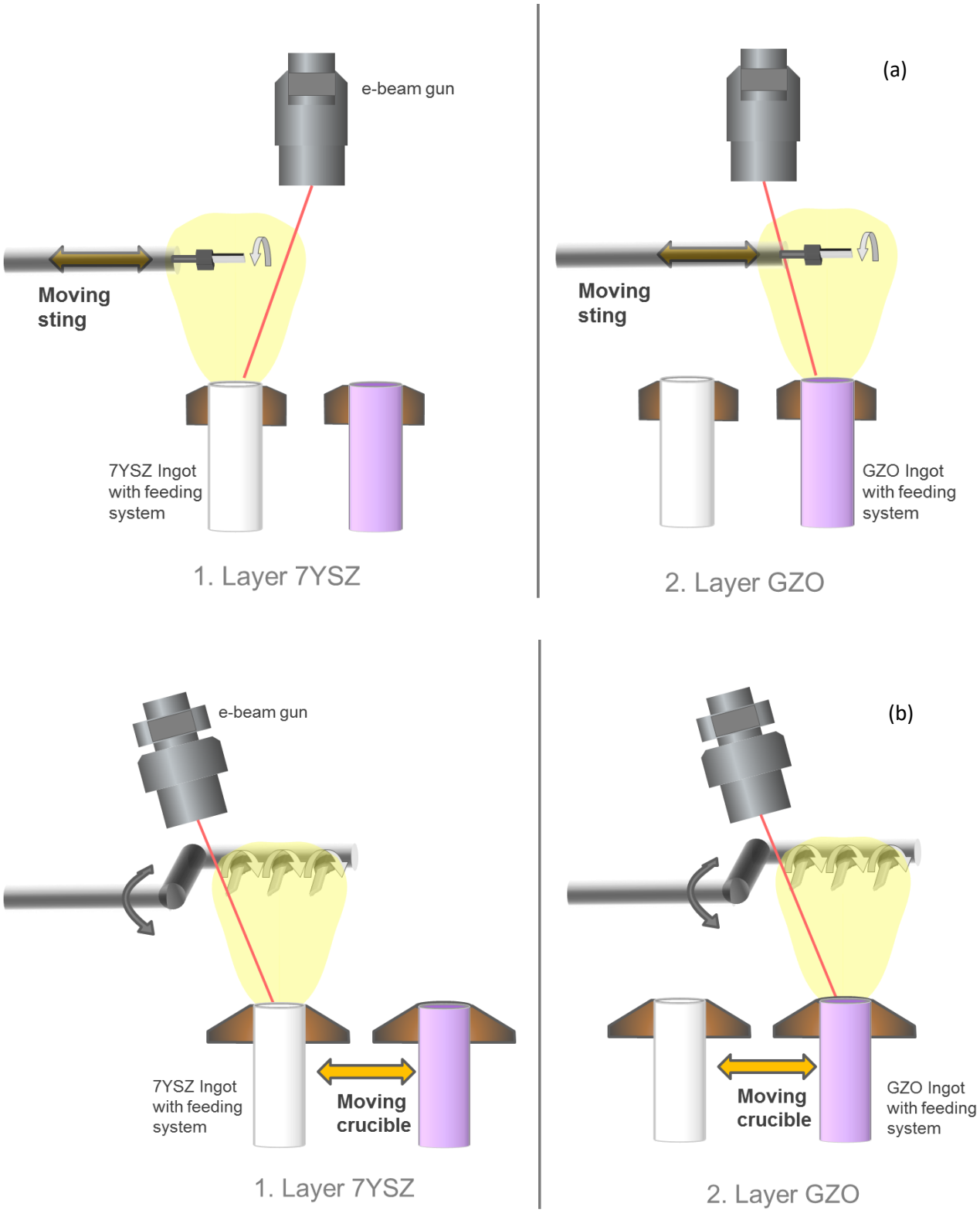


Figure 2: Sketch of the arrangement of the two crucibles, electron beam gun, and part holder in the evaporation chambers. (a) ESPRI using moving sample holder, and (b) SMART coater using moving crucibles.

The main process parameters used in the two different coaters for the deposition of the ceramic layers are summarized in Table 1.

Table 1: Summary of processing conditions and set up of the two coaters SMART and ESPRI

| Topic | SMART Coater | ESPRI |
|---|---|---|
| **Rotation of parts with regard to ingot axis** | 90°; tilting possible but not used, 10 rpm | Parallel, no tilting, 12 rpm |
| **Distance between crucibles and middle of rotational axis** | 375 mm | 335 mm |
| **Change of evaporation between two crucibles** | Moving crucibles | Moving sample holder (sting) |
| **Sample fixture** | 3 positions, variable holder | Planetary drive (cylinders) or holder for flat samples |
| **Typical ingot feed rate** | 1.6 to 1.9 mm/min | 1.0 to 1.5 mm/min |
| **Deposition rate** | similar | |
| **Pre-heating time and temperature under vacuum** | 20 minutes into standby heated chamber; 1050°C | 10 minutes into hot heating chamber; 950 to 1000°C |
| **Substrate temperature range applied in the experiments** | 940 – 1050°C | 990 – 1030°C |
| **Gases in coating chamber** | $O_2$ + some Ar | $O_2$ |
| **Pressure in coating chamber and vacuum pumps** | $10^{-3}$ to $10^{-2}$ mbar, diffusion pump | $10^{-3}$ to $10^{-2}$ mbar, turbo pump |
| **Total power used for evaporation** | 100 to 120 kW | 65 to 75 kW |

Pre-heating of the samples, rotation speed, distance between the two crucibles and between crucible level and rotational axis, overall pressure in the coating chamber, and the finally achieved deposition rates are quite similar in both coaters. Differences in the coating procedures comprise of the mode of rotation, position of the sample rotation axis with regard to

the ingots, the e-beam power used for evaporation, and the atmosphere within the coating chamber. Among others, the difference in total e-beam power used for evaporation originates from different electron gun types, scan patterns, heat dissipation in the evaporation plane, geometric conditions in the two different coating chambers, and different high voltage supply concepts. In both cases it was optimized to get similar evaporation conditions of the ingots. It must be noted that optimizing the whole pre-treatment procedure, such as bond coat annealing conditions and pre-heating of samples in the EB-PVD coater, was not the main focus of the current study but parameters were rather based on existing best practice used for 7YSZ coatings. Ingots of the same manufacturer (Phoenix coating Resources Inc, now a subsidiary of Saint-Gobain Coating Solutions, France) having a diameter of 62.5 to 62.9 mm were used in both coaters.

In order to study the effects of the interface between the two ceramic layers on lifetime and microstructure, a variety of ceramic bilayer top coats was deposited in addition to the reference single layer 7YSZ and single layer GZO. The 7YSZ layers were standard 7 wt% yttria stabilized zirconia while the GZO had an average composition of 59.5 to 61.5 wt% $Gd_2O_3$ + zirconia (including always traces of $HfO_2$) which is quite close to the intended 59.5 wt% $Gd_2O_3$ representing $Gd_2Zr_2O_7$.

Runs D, E, and ES produced single layers while all other were bilayers. The bilayers consisted of a 7YSZ base layer and the GZO top coat, respectively. All bilayers but F were produced in a single run that consisted of various stages. The characteristics of each run and the notation of the versions are listed in Table 2. Fast switch denotes a nearly immediate switch of the e-beam power from the 7YSZ to the GZO crucible (version B and BS). The slow transition included a period where the power was gradually increased on the GZO ingot while simultaneously the power was lowered on the 7YSZ ingot without changing the total e-beam power (version A and C). For version A the power transition from the 7YSZ to the GZO ingot was done first while the movement of the samples was done later, denoted as GZO deposition in stage 3 followed by a delayed sample motion from the position centered above the 7YSZ ingot to the position above the GZO ingot in stage 4.

*Table 2: Process conditions for all coating versions*

| **version** | **A** | **B** | **C** | **D** | **E** | **F** |
|---|---|---|---|---|---|---|
| **coater** | ESPRI | ESPRI | ESPRI | ESPRI | ESPRI | ESPRI |
| **Characte-risitic** | Bilayer | Bilayer | Bilayer | Single layer GZO | Single layer 7YSZ | Bilayer in two separate runs |
| **1st stage** | 7YSZ deposition | 7YSZ deposition | 7YSZ deposition | GZO deposition | 7YSZ deposition | 7YSZ deposition |
| **2nd stage** | slow transition from 7YSZ to GZO | fast switch from 7YSZ to GZO, sample motion (in parallel) | slow transition from 7YSZ to GZO, sample motion (in parallel) | | | removal from loading chamber, storage |
| **3rd stage** | GZO deposition | | | | | GZO deposition |
| **4th stage** | (delayed) sample motion | GZO deposition | GZO deposition | | | |

| **version** | **BS** | **ES** |
|---|---|---|
| **coater** | SMART | SMART |
| **Characte-risitic** | Bilayer | Single layer 7YSZ |
| **1st stage** | 7YSZ deposition | 7YSZ deposition |
| **2nd stage** | fast switch from 7YSZ to GZO, movement of crucibles (in parallel) | |
| **3rd stage** | | |
| **4th stage** | GZO deposition | |

Data of version D, E, and F are taken from [6]

Due to intended variations in the processing conditions, the layer thicknesses that are listed in Table 3 vary slightly. The total thickness of the TBCs was in the range between 150 and 180µm for all samples and therefore suited to compare the lifetimes without biasing the data by thickness fluctuations. The present differences in thickness are small for EB-PVD TBCs with respect to lifetime since even larger differences in 7YSZ top coat thickness between 60 and 370µm do not alter the FCT lifetime much [20]. The 7YSZ base layer thickness of 25 to 35 µm was also chosen to be the same for all versions with the exception of version BS.

Table 3: Thickness of the TBC layers. Numbers give the average values while the measured thicknesses varied by +/- 5µm. Version E was taken from earlier studies [21] based on a larger number of samples originating from various deposition runs. Therefore, the variation in thickness was in this case +/-15µm.

| **version** | **Thickness 1st layer (µm)** | **Thickness 2nd layer (µm)** |
|---|---|---|
| A | 35 | 145 (including 40 µm in first position) |
| B | 30 | 135 |
| BS | 82 | 80 |
| C | 25 | 145 |
| D<br>E<br>ES | 160<br>165<br>132 | |
| F | 25 | 160 |

All top coat depositions of the current study have been carried out at a substrate temperature of around 1000°C by using single and double source evaporation. The deposition rate of the bilayer runs in ESPRI was between 4.6 and 4.8 µm/min which is slightly lower than that of a pure 7YSZ layer which was in the order of 5 to 6 µm/min. In the SMART coater a deposition rate of 6 to 7 µm/min was applied.

Furnace cyclic testing (FCT) of the samples has been performed by a holding period in a pre-heated furnace at 1100°C for 50minutes and then forced air cooling for 10minutes, reaching nearly room temperature. Failure of the TBC systems was defined as the spallation of a top coat area with dimensions greater than 10mm. Since a variety of other substrates and bond coats have been investigate in parallel to this study in the same runs, mainly for microstructure examinations and other purposes, only a limited number of samples were available for FCT testing. Versions D, E, F, BS, and ES consisted of three samples each, version A of two samples and version B and C only of one single sample that was tested.

For cross-sectional investigations, cylindrical samples were cut and prepared by standard metallographic techniques. The microstructural analysis has been done in an analytical SEM (Zeiss DSM Ultra 55) equipped with an energy dispersive x-ray spectroscopy (EDS) system.

## 3. Results

### 3.1. Lifetime of the TBCs

The average lifetime of all versions tested under cyclic conditions of 50 minutes heating at 1100°C followed by 10 minutes cooling is shown in Figure 3. Within the uncertainties of a low number of samples for some versions and resulting weak statistics, the following conclusions are obvious.

(i) The 7YSZ TBCs had a comparable lifetime in both coaters.

(ii) All bilayers exhibited a longer lifetime with the exception of one very early failure for version A.

(iii) Both versions that were produced by a fast switch of the power from 7 YSZ to GZO during EB-PVD, i.e. versions B and BS, showed a longer lifetime than the other bilayers. This increase in lifetime was around 2.5 fold in both coaters.

Although the individual layer thicknesses are not fully comparable for those versions, it is remarkable that the lifetime is also longer than for a bilayer produced in two separate runs (version F). The lifetime of a single GZO layer adopted from a previous publication [6] on the same substrate - bond coat combination (version D) was around 50% higher than the best bilayer of the current study.

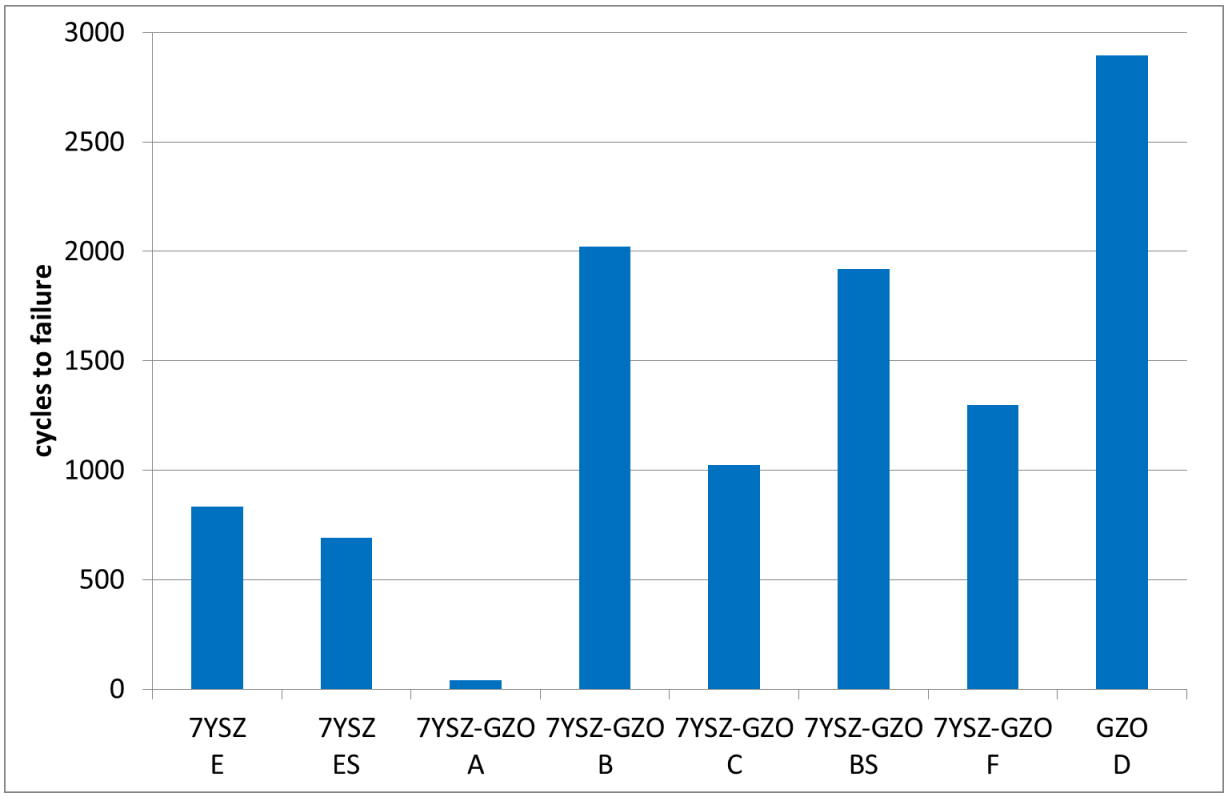


Figure 3: Lifetime in furnace cycle testing at 1100°C of the TBC versions investigated. Reference data of version E were taken from [21] and those of version D from [6].

### 3.2. Microstructure and failure behavior of the TBCs

All versions but A failed in the classical "black failure" regime either at the interface between 7YSZ and TGO or between TGO and bond coat with some regions on the samples showing a mix of those two locations. Version A failed in a "white failure mode" between 7 YSZ and GZO, see Figure 4. While all the thicker GZO layers deposited in the coater ESPRI showed indications of column bending that was previously identified to originate from the direction of rotation [6, 19], version BS from the SMART coater did not show any signs of column bending (Figure 5). The different direction of bending observed for the ESPRI bilayers originated from the view direction on the cross section with regard to the rotation direction; see differences in bending in Figure 5 (a) and (b). The GZO columns in the bilayers of ESPRI grew similar to the single layer version D, but showed some differences to 7YSZ. As previously investigated [6], GZO columns have a higher propensity to column diameter enlargement in the upper TBC region, regardless of single or bilayer architecture. Interestingly, most GZO TBC where white after deposition but turned into light brownish-purple color after short testing intervals. The reason behind that is still unknown but was not within the focus of this study.

(a)

(b)

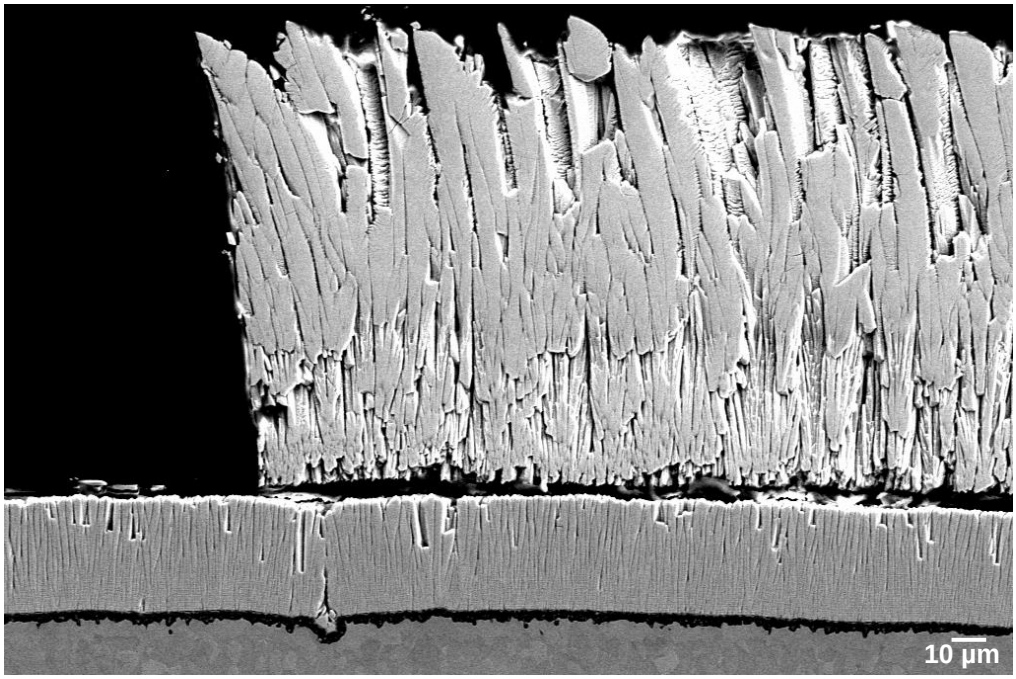


(c)

Figure 4: Failure location of version A: (a) and (b) macroscopic pictures after 40 cycles, and (c) crack formation and propagation between 7YSZ and GZO after 40 cycles in SEM cross section.

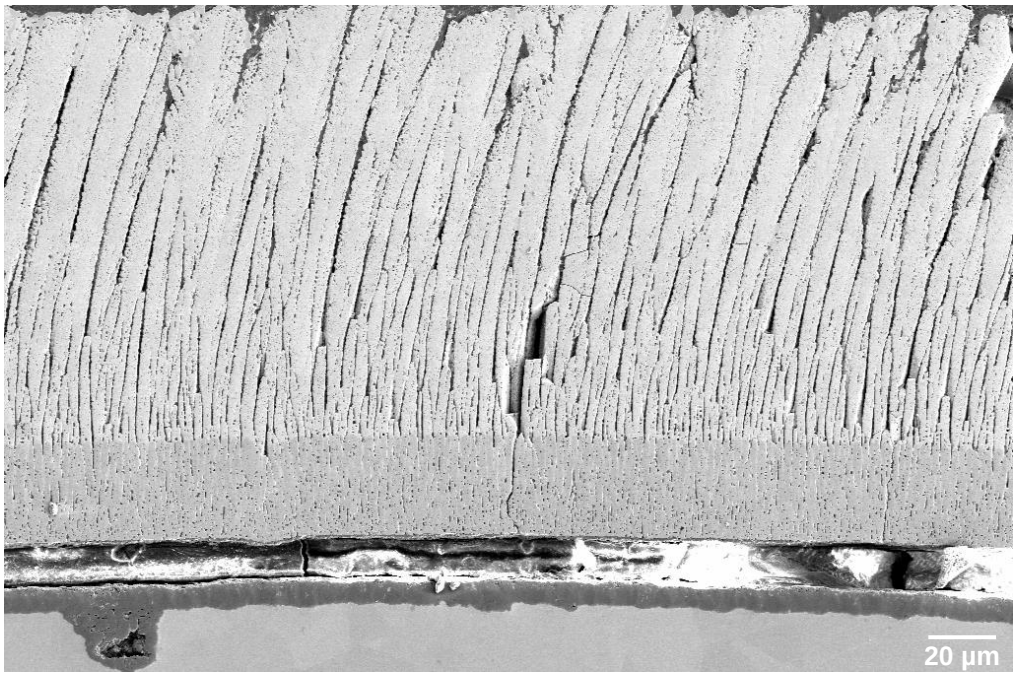


(a)

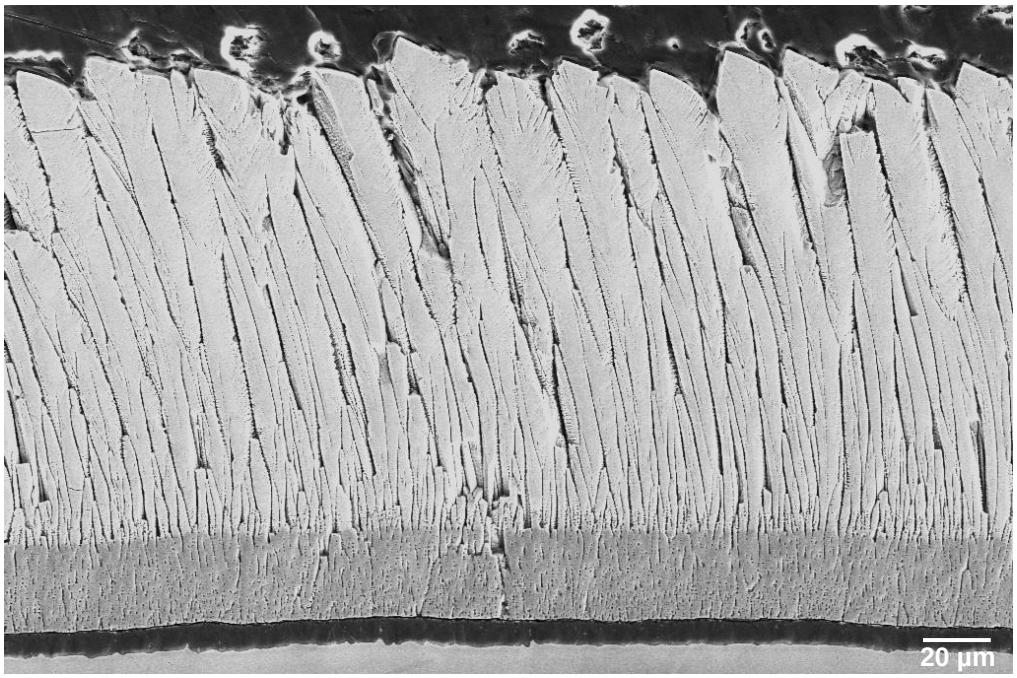


(b)

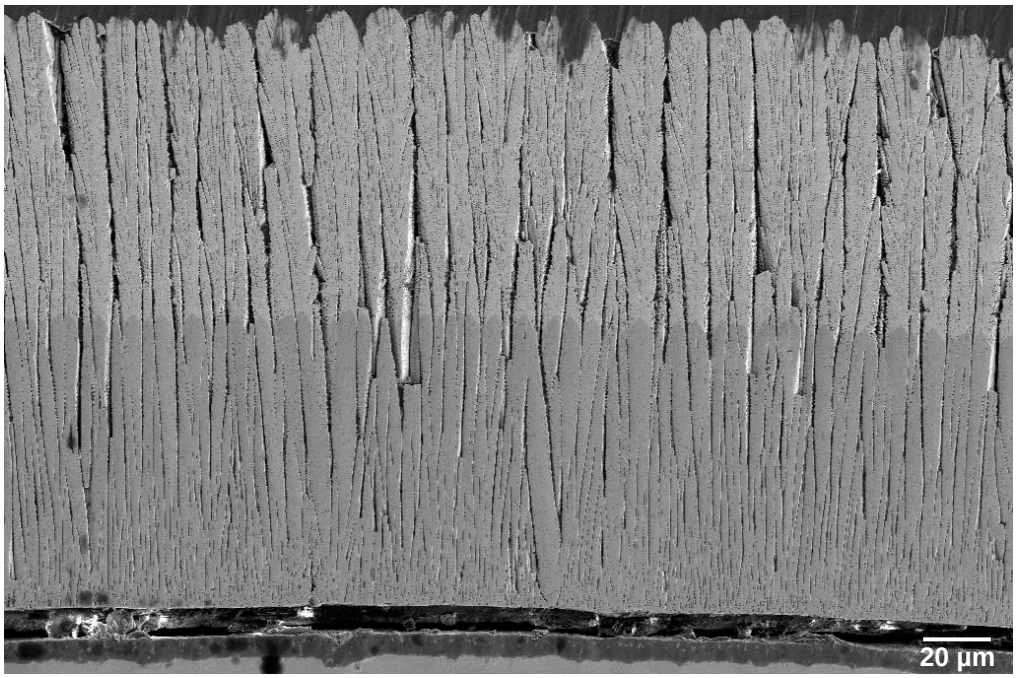


(c)

Figure 5: Failure location of the bilayer TBCs having a longer life time, and overview of microstructures in cross section. (a) Version B failure location mainly between 7YSZ and TGO after 2021 cycles, (b) version C failure location mainly between 7YSZ and TGO after 1023 cycles, and (c) version BS failure location between 7YSZ base layer and TGO after 1337 cycles.

Special emphasis was put on the interface between the two ceramic top layers. The striking differences between the interfaces are shown in Figure 6. For all versions the growth of columns is nearly continuous across the 7 YSZ to the GZO layer. Columns are merging from the 7YSZ into the GZO without notable interruption or change in shape, i.e. the column diameter and number does not change at this interface. Version A is characterized by an accumulation of porosity within the first layers of the GZO. All other bilayer versions do not show this accumulation of porosity, regardless of the coater. After extended testing time, signs of TBC sintering become visible, leading to pore coarsening (see Figure 6 (c) to (f)). Some inter-diffusion mainly of the gadolinium into the 7YSZ and especially along the inter-columnar gaps within the base layer was observed and verified by EDS (see circled areas in Figure 6 (e) and (f)).

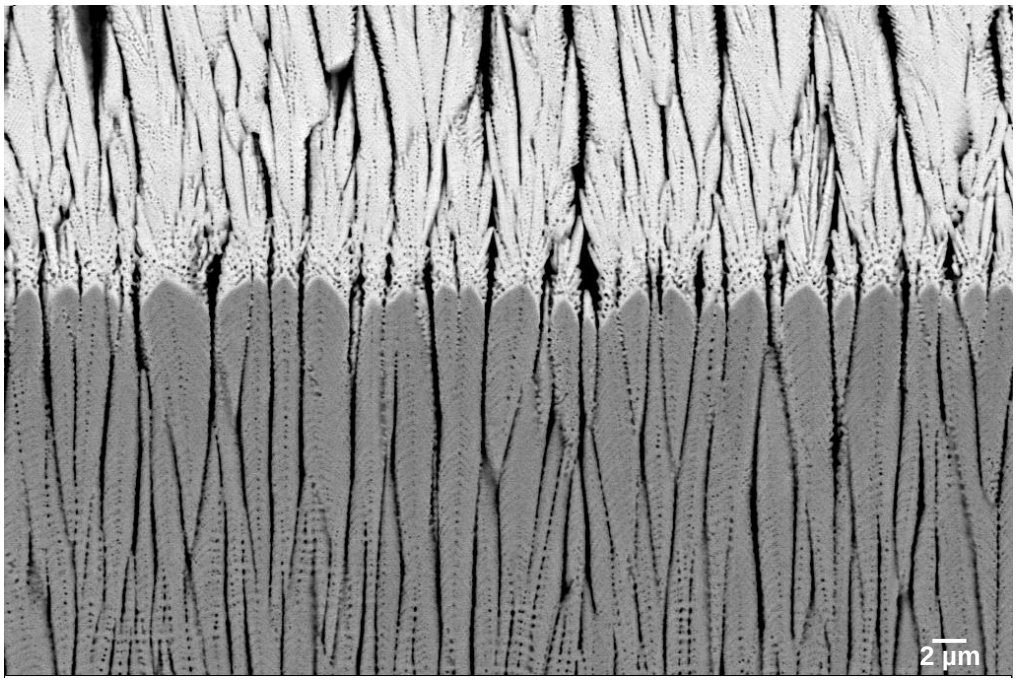


(a)

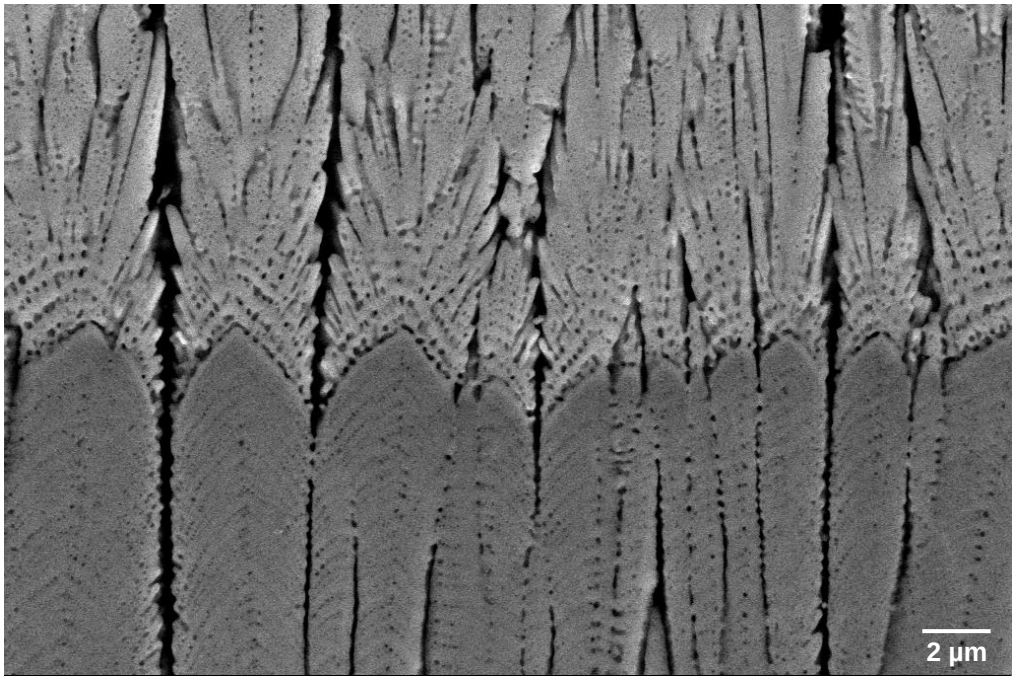


(b)

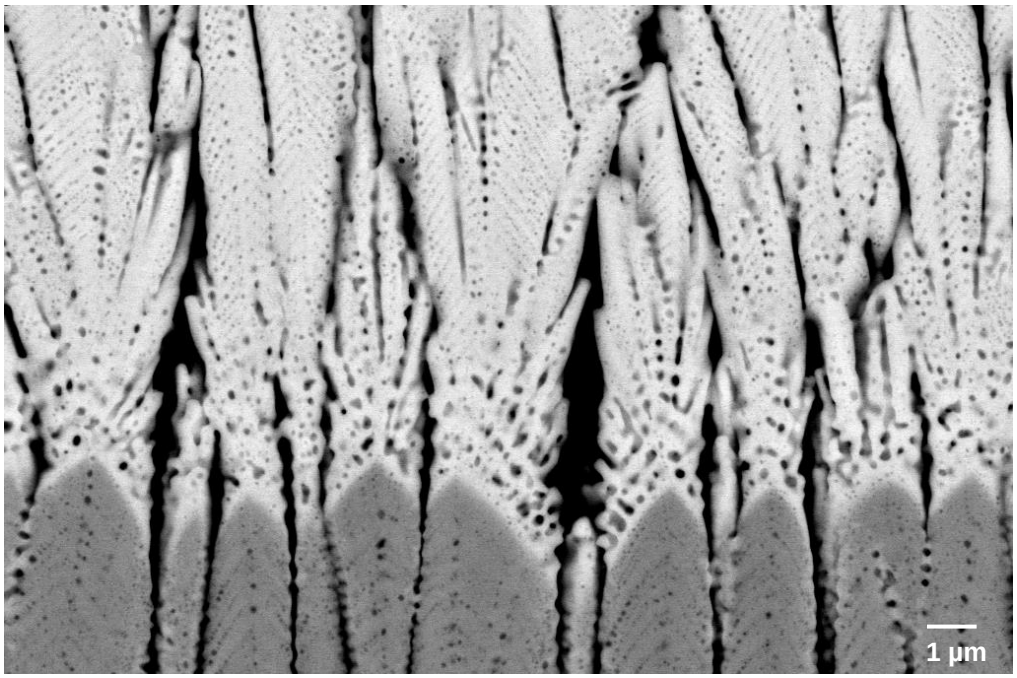


(c)

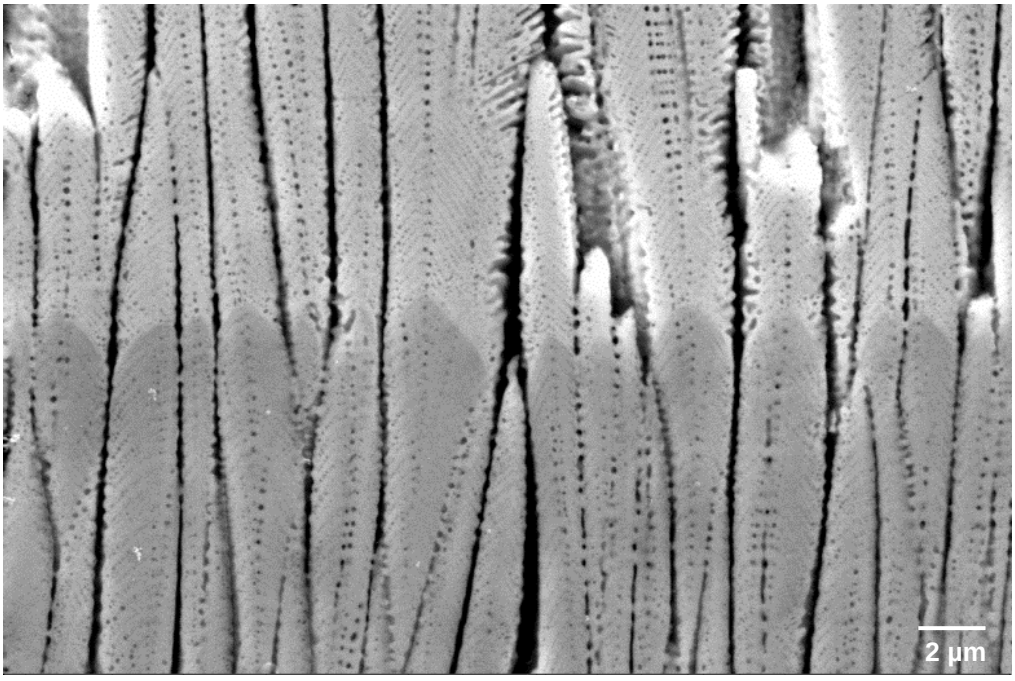


(d)

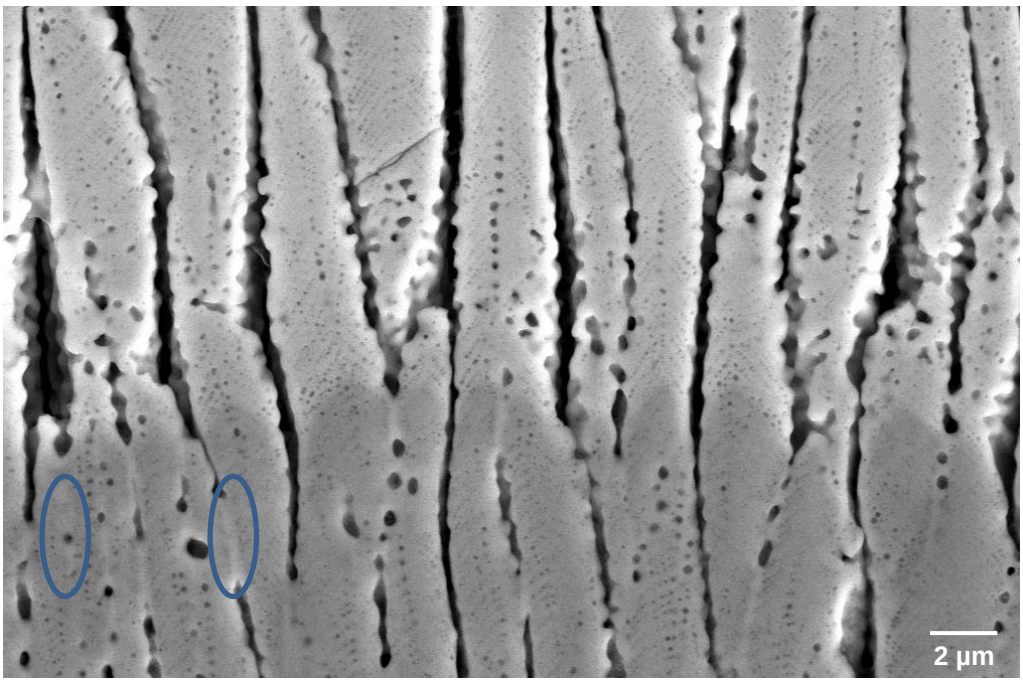


(e)

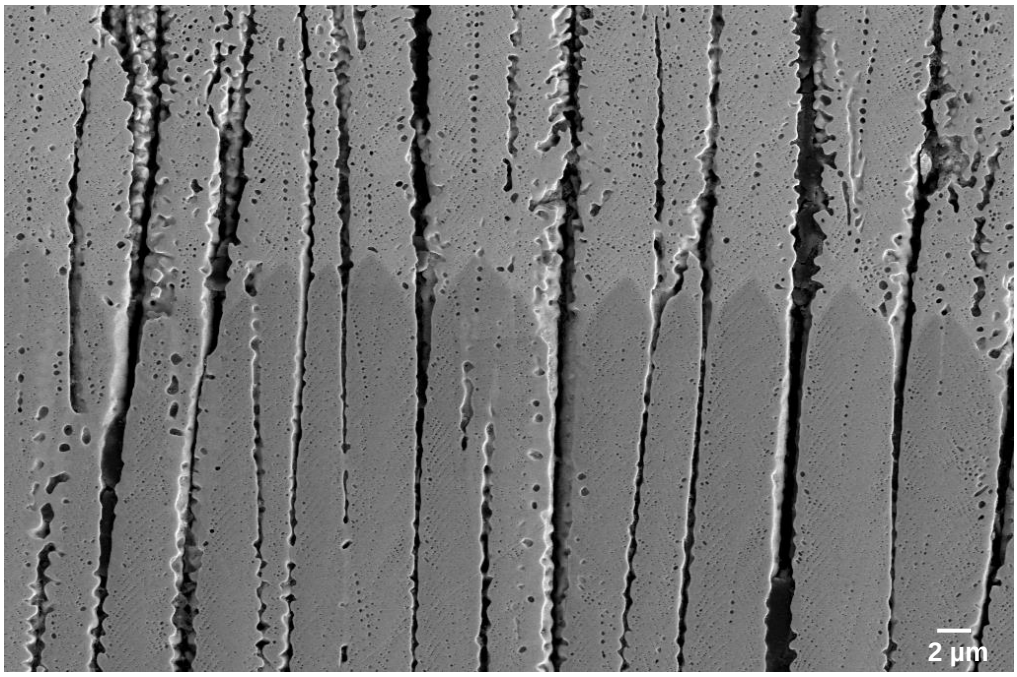


(f)

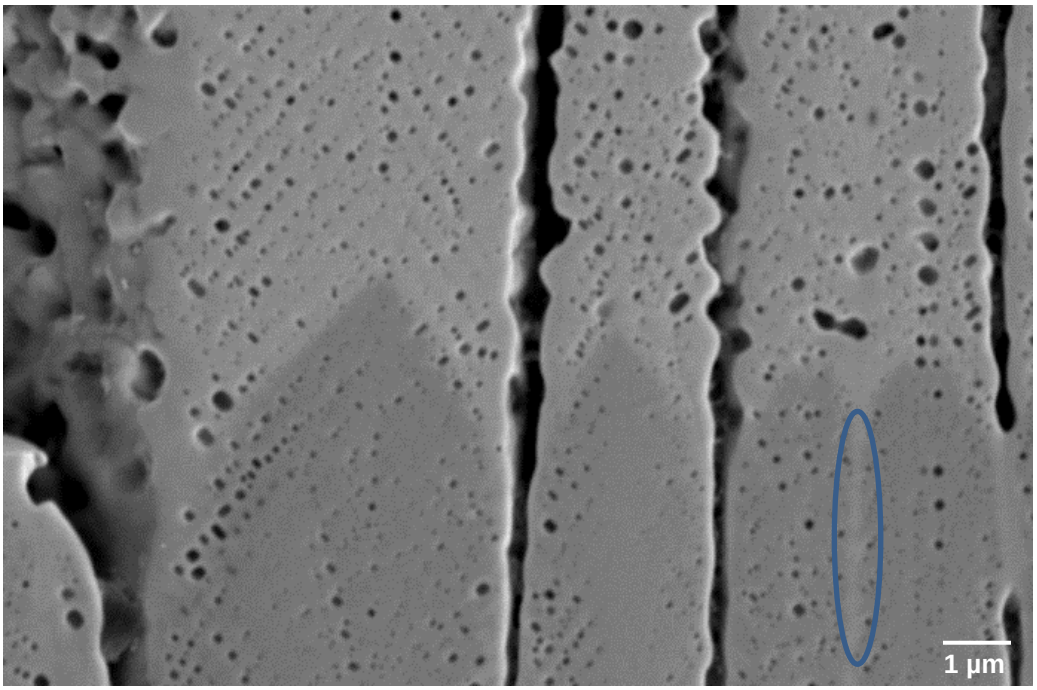


(g)

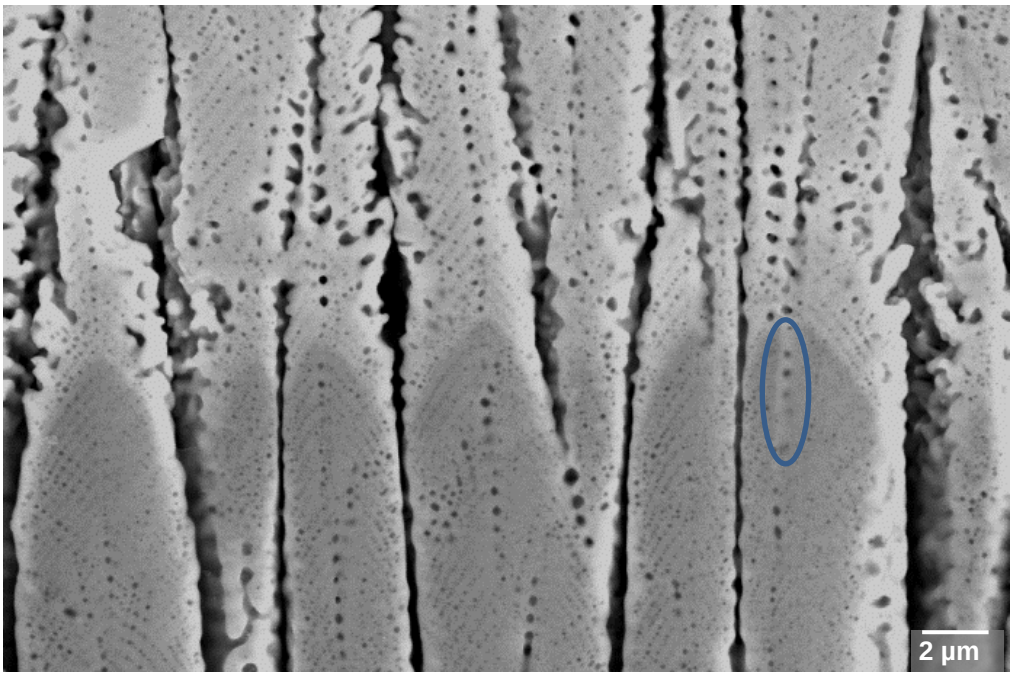


(h)

Figure 6: High magnification SEM cross sections of the interface between 7 YSZ and GZO layer. (a) to (c) version A after 60 cycles, (d) version B after 40 cycles, (e) version C after 1023 cycles, (f) and (g) version BS after 1337 cycles, and (h) version BS after 1024 cycles. Circled areas indicate presence of gadolinium within the 7YSZ layer which was verified by EDS spot measurements.

### 3.3. TGO formation during testing

TGO formation for all systems that have a first 7 YSZ layer on top of the bond coat was similar. As commonly observed for this type of bond coat, the TGO consisted of alpha alumina with some yttrium-rich inclusions that were mainly identified as Y-aluminates such as YAG (garnet) and YAP (perovskite) in previous work [22, 23] and confirmed by EDS in this work as well, see Figure *7*. Exclusively Y, Al and O are present in those particles. The TGO grew in thickness from around 2µm after 40 cycles up to 7 µm after 1000 cycles and only slightly thickened up to 8µm after 2000 cycles. TGO thickening was quite similar for all versions and was similar to the growth behavior previously observed for this NiCoCrAlY bond coat. Only in very limited areas the TGO grew already locally thicker after TBC deposition in a kind of protrusion as shown in Figure 4c) and Figure 5a) which is mainly caused by remaining small defects or undulations of the bond coat after peening.

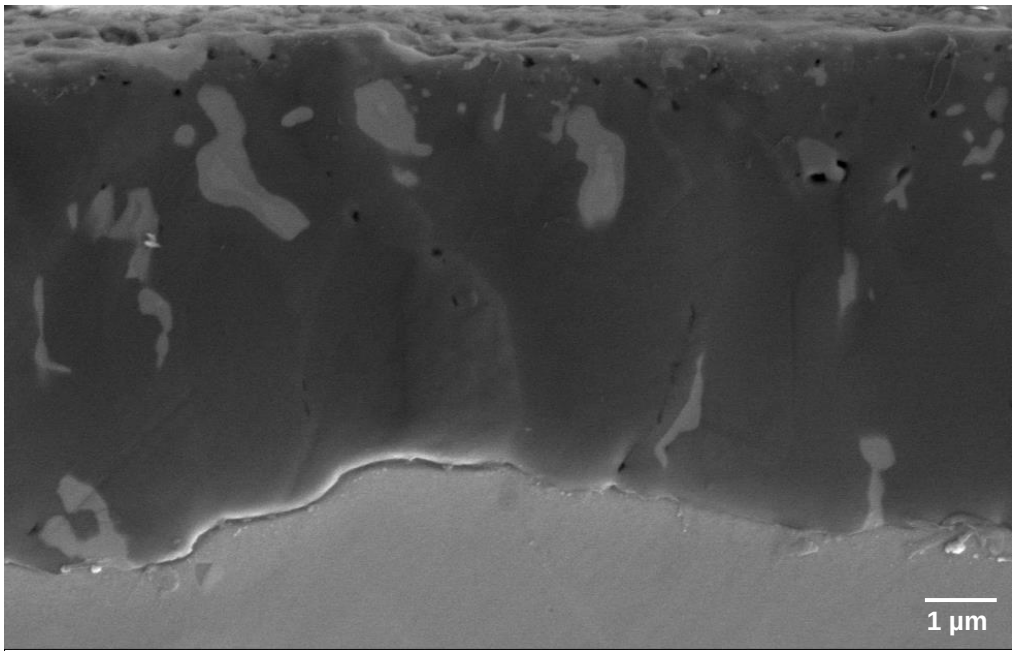


Figure 7: Example of TGO formation in systems having a 7YSZ base layer; version BS after 1337 cycles

The TGO growth of version D (pure GZO) was briefly introduced in [6]. In summary, alpha alumina forms including the Y-aluminates described above at a similar growth rate as for 7YSZ. The striking difference is a slowly progressing reaction between alumina and gadolinium-zirconate with time at temperature since both phases are not in equilibrium when in

contact to each other. This interface and the phases that form are currently investigated by TEM in detail which is the subject of a forthcoming paper.

## 4. Discussion

The lifetime of 7 YSZ single layers (versions E and ES) is similar in both coaters despite of small variations in processing conditions. This indicates that the standard TBC investigated on the IN100 Ni-based superalloy substrate with an EB-PVD NiCoCrAlY bond coat and adequate pre-treatment prior to TBC deposition is a robust coating system capable of being manufactured under a variety of EB-PVD processing conditions.

Nearly all research on air plasma-sprayed and suspension plasma-sprayed GZO layers reveals a superior lifetime for bilayer TBC in comparison to single layers of GZO or 7YSZ [3, 4, 14, 24-26]. Such bilayers are now the standard for those coatings. However, only limited and varying information is available for EB-PVD coatings. A long lifetime of $Gd_{0.9}Yb_{0.1}$-zirconat bilayers under thermal shock testing is reported by Guo et al. [27], unfortunately, without a comparison to the lifetime of standard single 7YSZ layers. For TBCs having a coarse-columnar and more cauliflower-like microstructure deposited under low temperature EB-PVD conditions the following results were found: bilayers 7YSZ/GZO of the same layer thickness possessed a slightly longer lifetime than single layers of 7 YSZ or GZO that had nearly the same lifetime [7]. Early spallation of GZO single layers was observed by Bobzin et al. [28] under short isothermal testing at 1300°C while bilayer 7YSZ/GZO and single 7YSZ did not spall. The lifetime of bilayer Samarium-zirconate coatings manufactured by electron-beam directed vapor deposition (EB-DVD) was reported to be four times higher than that of pyrochlore single layers under FCT at 1100°C [29], but in a similar range to that of single 7 YSZ layers.

Most bilayers of the current study exhibited a longer lifetime than the 7YSZ base line coating (within the limits of low sample numbers for some versions and implications for statistics). Only version A suffered from early TBC spallation and an unusual “white failure” mode by spallation of the GZO layer at the interface to the 7YSZ base layer that was still attached to the bond coat, see Figure 4. The reason for this failure location is the pore formation in the root area of the GZO layer that originated from the mode of transition between the two layers. While the transfer of the e-beam power from the 7YSZ to the GZO crucible was done properly but slowly, the motion of the samples was intentionally delayed. The layers that originate from each rotation due to the well-known sunset-sundown vapor flux impinging on the surface [30,

31] exhibit much larger pores in the GZO base zone than usual. In some areas and on some 7YSZ columns the column diameter becomes even smaller within this first GZO area of around 2 to 3 µm which represents 4 to 6 revolutions, leading to enhanced porosity between the columns. This means that locally, the inter-columnar gaps are larger. The delayed sample motion introduced a longer period of a heavily inclined vapor incidence angel (VIA) of the GZO vapor stream impinging on the substrate surface that surprisingly did not initiate column inclination. In addition, the deposition rate in stage 3 was smaller, and most likely the temperature may have been slightly lower as well. The pores and larger inter-columnar gaps arranged parallel to the surface clearly represent a weak area within the TBC. This provides an easy crack path through the zone of reduced mechanical strength within the root area of the GZO layer. An additional weak area within the GZO layer was found at the region of transition between the inclined and regular deposition (90° VIA) that shows indication of crack formation during metallographic preparation, but no spallation during FCT.

Comparing the performance of the other bilayers (B, C, F, and BS) it is obvious that a fast switch of the e-beam between two ingots seems to be favorable. Version B and BS exhibited a considerable longer lifetime than the version deposited under a slow power transition (version C) or in two separate runs (version F). Surprisingly, the interfaces of those “fast switch” versions did not show a different microstructure under careful SEM investigation. The ultimate reason for those variations in lifetime could not be identified in this study since all versions described above spalled at the interface between the 7 YSZ layer and TGO or between TGO and bond coat which indicates that minor variations in the transition between the 7 YSZ and the GZO layer are less important for failure localization. The low number of samples of versions B and C may have overshadowed the statistical relevance of the lifetime data as well. As elaborated by Jackson et al. [16], under thermal gradient conditions present during the heating and especially the cooling phase in FCT used in the this study, the lower thermal conductivity of GZO may have changed the temperature profile across the whole cylindrical sample and consequently the transient stress state. This could have influenced the energy release rate for delamination which could explain the longer lifetime of the bilayers found here. Again, the lifetime of versions B and BS that were manufactured in a similar manner but using different coaters is nearly the same. Even the differences in the mode of transition of beam power from 7YSZ deposition to GZO deposition including both crucibles movement or sample movement, and variations in vapor stream arrangement with respect to the main sting and sample rotation axis did not alter the lifetime. In other words, it is of less importance whether the crucibles are moved together with the electron beam pattern and samples are rotated in a fixed position

(SMART coater) or the crucibles are fixed and both electron beam pattern and samples are moved as applied in the (ESPRI coater). The failure location of bilayers in the current study with mostly failure along the TGO is in agreement with findings in [29] and [7], while failure between the GZO and 7YSZ as found here only for version A is similar to reports given by Zhang et al. [32] and Guo et al. [27]. Most reports for thermally sprayed bilayer TBCs describe failure at or above the interface between the two ceramic layers, especially under thermal shock conditions applying a temperature gradient across the sample thickness [4, 14].

The single layer GZO from a previous study [6, 19] (version D) still outperforms both double and 7YSZ single layers, showing the highest lifetime of nearly 3000 cycles on the substrate - bond coat combination used in this study. A similar prolonged lifetime was found with GZO single layers in comparison to 7YSZ layers on single crystal substrates, i.e. a much longer life of the GZO if the same NiCoCrAlY bond coat is applied [5]. Only when the bond coat composition was changed to an Hf-doped NiCoCrAlY, the lifetimes of both versions further increased but in the end they were similar and high. It is worth mentioning that testing under temperature gradient conditions may give other results since the stress situation is different and a bilayer may benefit from the higher fracture toughness of the 7YSZ base layer.

No major differences in TGO formation and thickening over time were observed for all bilayers in comparison to pure 7 YSZ. This was expected since the 7 YSZ base layer acts as a “glue” and buffer layer between the less tough GZO and the TGO, hence TGO growth is not influenced by the GZO layer that is 25 to 35 µm distant from the TGO. The limited diffusion of Gd into the 7 YSZ layer found in the present experiments was restricted to local areas, especially along former inter-columnar gaps that had sintered together during prolonged high temperature exposure (see Figure 6 (e) and (f)). The diffusion distance is only some µm and it does not influence TGO growth or adhesion in the present case. This limited upward diffusion is in agreement with our previous results for version F [6] as well as findings in literature [7]. Results presented by Zhao et al. [29] suggest that the base layer should be thicker than 10µm. For bilayers of only 10µm 7 YSZ plus 80µm Sm-zirconate deposited by EB-DVD a limited diffusion of the Sm cations into the 7YSZ base layer was in analogy observed along inter-columnar gaps. After 350 hrs at 1100°C in FCT gadolinium has partially diffused through the thin 7YSZ layer to the TGO. Therefore, from a chemical point of view, a 7YSZ base layer thickness in the order of 30µm is sufficient while mechanical considerations may favor a variant thickness as elaborated by Jackson et al. [16].

Finally, some aspects of the TBC microstructure are discussed. Column bending within the GZO layers occurs only under certain parameter combinations that are still not identified. This implies that column bending for GZO is highly sensitive to the process parameters. Most likely the mode of rotation with regard to ingot position in combination with deposition rate, chamber pressure, and substrate temperature play an important role. Additional deposition runs in the SMART coater on different substrate bond coat combinations performed to produce a similar thin 7YSZ base layer of around 35 µm and a 120 µm thick GZO top layer did also not show any bending. This precludes the GZO layer thickness as an important factor for column bending.

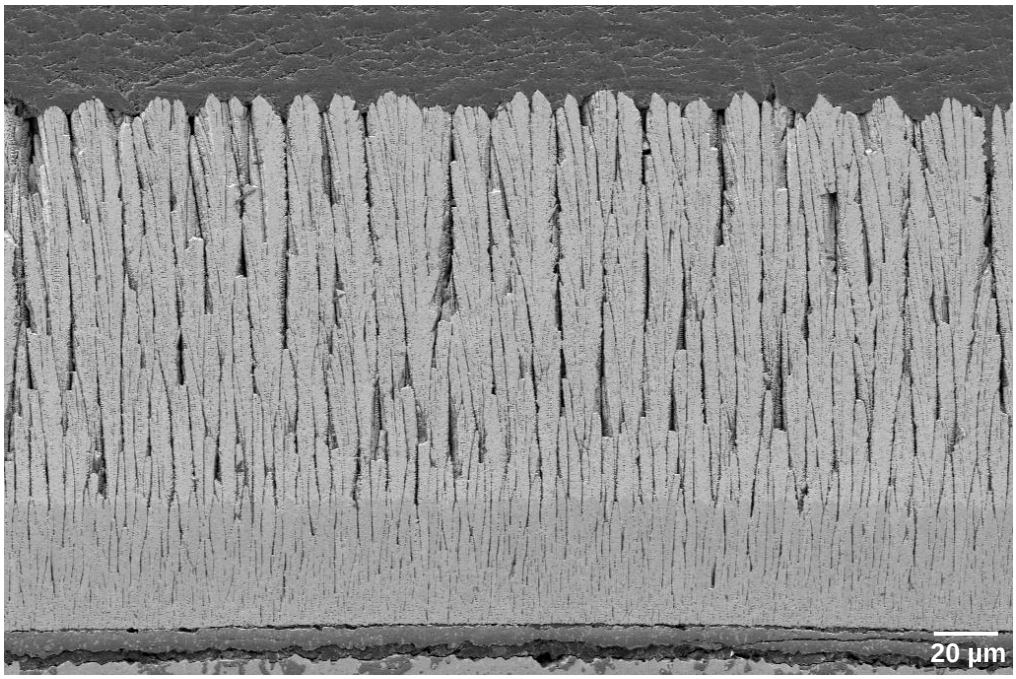


Figure 8: A modified version of BS manufactured in a separate run applying a thin 7YSZ base layer and a thick GZO layer on a CMSX-4 substrate after 322 cycles, indicating a straight growth of the bilayer columns.

Whenever the interface between the 7YSZ and GZO layer is generated properly (all versions but A), the GZO growth in a bilayer is quite similar to the growth of a single layer. In those cases the 7YSZ layer acts as a template for the growth of the superjacent GZO layer, i.e. the columns all grow through and do not change in thickness or number at this interface. This is identical to findings for 7YSZ layers that were originating from three separate interrupted runs [33] where columns grew through from one layer to the next without any interruption. Only minor variations in porosity were found in this study at the interface regions. Similarly, bilayers

of 7YSZ and Dy-stabilized zirconia deposited in two separate runs showed the same growth behavior without interruption of the columnar growth [6]. In other studies, even when the deposition conditions did not allow a favorable regular columnar growth and by using Lanthanum -zirconate [18] or Lanthanum-Cerium-zirconate [34] as top coats that both always suffer from fluctuation in chemistry, no interruption in the columnar growth between the 7YSZ base layer and the top layer was observed as well. The same templating effect of EB-PVD bilayers was observed when coatings for CMAS protection where applied on top of relatively thick 7 YSZ acting as the main layer. This was found e.g. for alumina [35] and for pure yttria and 65wt% yttria – zirconia [36]. In essence, the current results clearly show that bilayer TBCs can be manufactured by EB-PVD in a variety of ways with a preference for non-interrupted deposition of the two layers.

## Conclusions

This research was performed to elucidate the role of different EB-PVD coaters and the design of the interface between a 7YSZ base layer and a Gadolinium-zirconate (GZO) top layer on microstructure and lifetime of single and bilayer TBCs. The results reveal that:

- The single layer 7YSZ baseline coating is a robust system in EB-PVD processing, and similar lifetimes have been achieved in two different coaters under slightly varying processing conditions.

- When a proper interface between 7YSZ and GZO is manufactured, longer lifetime of bilayers compared to 7YSZ layers can be achieved in Furnace Cycle Testing. A fast switch of the e-beam power between evaporation sources seems to be favorable since a similar longer lifetime was achieved in both coaters for the best bilayers manufactured in non-interrupted runs. Both moving crucibles / fixed sample rotation and fixed crucibles / moving samples seem to work properly for the transition between the layers.

- A favorable interface between 7YSZ and GZO facilitates continuous column growth across base layer and top layer, i.e. without interruption of the columnar growth. A templating effect induces GZO growth with initially the same column geometry as the underlying 7YSZ.

- Long periods of inclined vapor incidence angles should be avoided since they can trigger formation of pores and larger inter-columnar gaps at the interface between 7YSZ and GZO, leading to easy crack propagation and early failure of the TBC.

- There is only limited inter-diffusion between both layers; mainly Gd diffuses along inter-columnar gaps into 7YSZ. A 25 to 30µm thick base layer is sufficient to prevent any change in TGO growth and provides similar TGO behavior as in single 7YSZ layers.

- The longest lifetime was achieved for single layer GZO regardless of the limited reaction between GZO and TGO. Since the phases grew very slowly and formed only a thin reaction zone of about 1µm after ~1500 hot hours at 1100°C, it is believed that they are not detrimental for the lifetime of GZO single layer TBCs.

**Acknowledgement**

The authors thank J. Brien, A. Handwerk and D. Peters from DLR for technical support and N. Laska and P. Mechnich for helpful discussions on the manuscript. The work was partly performed in the framework of the research project GOLETA (German-Polish Center of excellence for EB-PVD technology for aviation applications) funded by the German Federal Ministry of Education and Research. The work was also supported by the grant PBS1/A5/10/2012 of the National Centre for Research and Development Funds in Poland. The authors acknowledge the financial support.

## References


1. Krämer, S., et al., *Mechanisms of cracking and delamination within thick thermal barrier systems in aero-engines subject to calcium-magnesium-alumino-silicate (CMAS) penetration.* Materials Science and Engineering: A, 2008. **490**(1-2): p. 26-35.
2. Drexler, J.M., et al., *Plasma sprayed gadolinium zirconate thermal barrier coatings that are resistant to damage by molten Ca–Mg–Al–silicate glass.* Surface and Coatings Technology, 2012. **206**(19–20): p. 3911-3916.
3. Vaßen, R., et al., *Overview on advanced thermal barrier coatings.* Surface and Coatings Technology, 2010. **205**(4): p. 938-942.
4. Bakan, E., et al., *Gadolinium Zirconate/YSZ Thermal Barrier Coatings: Plasma Spraying, Microstructure, and Thermal Cycling Behavior.* Journal of the American Ceramic Society, 2014. **97**(12): p. 4045-4051.
5. Munawar, A.U., U. Schulz, and M. Shahid, *Microstructure and lifetime of EB-PVD TBCs with Hf-doped bond coat and Gd-zirconate ceramic top coat on CMSX-4 substrates.* Surface and Coatings Technology, 2016. **299**: p. 104-112.
6. Munawar, A.U., et al., *Microstructure and cyclic lifetime of Gd and Dy-containing EB-PVD TBCs deposited as single and double-layer on various bond coats.* Surface and Coatings Technology, 2014. **245**(0): p. 92-101.
7. Doleker, K.M., et al., *Evaluation of oxidation and thermal cyclic behavior of YSZ, Gd2Zr2O7 and YSZ/Gd2Zr2O7 TBCs.* Surface and Coatings Technology, 2019. **371**: p. 262-275.
8. Doleker, K.M. and A.C. Karaoglanli, *Comparison of oxidation behavior of YSZ and Gd2Zr2O7 thermal barrier coatings (TBCs).* Surface and Coatings Technology, 2017. **318**: p. 198-207.
9. Krämer, S., J. Yang, and C.G. Levi, *Infiltration-Inhibiting Reaction of Gadolinium Zirconate Thermal Barrier Coatings with CMAS Melts.* Journal of the American Ceramic Society, 2008. **91**(2): p. 576-583.
10. Levi, C.G., *Emerging materials and processes for thermal barrier systems.* Current Opinion in Solid State and Materials Science, 2004. **8**(1): p. 77-91.
11. Schulz, U., et al., *Review on Advanced EB-PVD Ceramic Topcoats for TBC Applications.* Int. J. Applied Ceramic Technology, 2004. **1**(4): p. 302-315.
12. Clarke, D.R. and S.R. Phillpot, *Thermal barrier coating materials.* Materialstoday, 2005. **June**: p. 22-29.
13. Leckie, R.M., et al., *Thermochemical compatibility between alumina and ZrO2-GdO3/2 thermal barrier coatings.* Acta Materialia, 2005. **53**(11): p. 3281-3292.

14. Mahade, S., et al., *Influence of YSZ layer thickness on the durability of gadolinium zirconate/YSZ double-layered thermal barrier coatings produced by suspension plasma spray.* Surface and Coatings Technology, 2019. **357**: p. 456-465.
15. Viswanathan, V., G. Dwivedi, and S. Sampath, *Multilayer, Multimaterial Thermal Barrier Coating Systems: Design, Synthesis, and Performance Assessment.* Journal of the American Ceramic Society, 2015. **98**(6): p. 1769-1777.
16. Jackson, R.W., et al., *Response of molten silicate infiltrated Gd2Zr2O7 thermal barrier coatings to temperature gradients.* Acta Materialia, 2017. **132**: p. 538-549.
17. Schmitt, M.P., et al., *Multilayer thermal barrier coating (TBC) architectures utilizing rare earth doped YSZ and rare earth pyrochlores.* Surface and Coatings Technology, 2014. **251**(0): p. 56-63.
18. Doleker, K.M., Y. Ozgurluk, and A.C. Karaoglanli, *Isothermal oxidation and thermal cyclic behaviors of YSZ and double-layered YSZ/La2Zr2O7 thermal barrier coatings (TBCs).* Surface and Coatings Technology, 2018. **351**: p. 78-88.
19. Munawar, A.U., U. Schulz, and G. Cerri, *Microstructural Evolution of GdZ and DySZ Based EB-PVD TBC Systems After Thermal Cycling at High Temperature.* Journal of Engineering for Gas Turbines and Power, 2013. **135**(10): p. 1021011-1021016.
20. Schulz, U., et al., *Factors affecting cyclic lifetime of EB-PVD thermal barrier coatings with various bond coats.* Zeitschrift f. Metallkd., 2003. **94**(6): p. 649-654.
21. Schulz, U., K. Fritscher, and A. Ebach-Stahl, *Cyclic behavior of EB-PVD thermal barrier coating systems with modified bond coats.* Surface and Coatings Technology, 2008. **203**(5-7): p. 449-455.
22. Braue, W., et al., *Analytical Electron Microscopy of the Mixed Zone in NiCoCrAlY-Based EB-PVD Thermal Barrier Coatings: As-coated Condition Versus Late Stages of TBC Lifetime.* MATERIALS AT HIGH TEMPERATURES, 2005. **22**(3-4): p. 393-401.
23. Braue, W., et al., *Compatibility of mixed zone constituents (YAG, YAP, YCrO3) with a chromia-enriched TGO phase during the late stage of TBC lifetime.* Surface and Coatings Technology, 2007. **202**(4–7): p. 670-675.
24. Viswanathan, V., G. Dwivedi, and S. Sampath, *Engineered Multilayer Thermal Barrier Coatings for Enhanced Durability and Functional Performance.* Journal of the American Ceramic Society, 2014. **97**(9): p. 2770-2778.
25. Mahade, S., et al., *Thermal conductivity and thermal cyclic fatigue of multilayered Gd2Zr2O7/YSZ thermal barrier coatings processed by suspension plasma spray.* Surface and Coatings Technology, 2015. **283**: p. 329-336.

26. Wang, L., et al. *Thermal Cycling Behavior of Gd2Zr2O7 Based Thermal Barrier Coatings*. in *MS&T Conference*. 2011. Columbus , OH.
27. Guo, L., et al., *Thermophysical properties of Yb2O3 doped Gd2Zr2O7 and thermal cycling durability of (Gd0.9Yb0.1)2Zr2O7/YSZ thermal barrier coatings.* Journal of the European Ceramic Society, 2014. **34**(5): p. 1255-1263.
28. Bobzin, K., et al., *Influence of temperature on phase stability and thermal conductivity of single- and double-ceramic-layer EB–PVD TBC top coats consisting of 7YSZ, $Gd_2Zr_2O_7$ and $La_2Zr_2O_7$.* Surface and Coatings Technology, 2013. **237**(0): p. 56-64.
29. Zhao, H., et al., *Reaction, transformation and delamination of samarium zirconate thermal barrier coatings.* Surface and Coatings Technology, 2011. **205**(19): p. 4355-4365.
30. Schulz, U., S.G. Terry, and C.G. Levi, *Microstructure and texture of EB-PVD TBCs grown under different rotation modes.* Materials Science and Engineering A, 2003. **360**(1-2): p. 319-329.
31. Terry, S.G., J.R. Litty, and C.G. Levi, *Evolution of porosity and texture in thermal barrier coatngs grown by EB-PVD*, in *Elevated temperature coatings: Science and technology III*2003.
32. Zhang, H., et al., *Thermal cycling behavior of (Gd0.9Yb0.1)2Zr2O7/8YSZ gradient thermal barrier coatings deposited on Hf-doped NiAl bond coat by EB-PVD.* Surface and Coatings Technology, 2014. **258**(0): p. 950-955.
33. Schulz, U., et al., *Thermal conductivity issues of EB-PVD thermal barrier coatings.* Materialwissenschaft und Werkstofftechnik, 2007. **38**(9): p. 659-666.
34. Shen, Z., et al., *LZC/YSZ DCL TBCs by EB-PVD: Microstructure, low thermal conductivity and high thermal cycling life.* Journal of the European Ceramic Society, 2019. **39**(4): p. 1443-1450.
35. Naraparaju, R., et al., *EB-PVD alumina (Al2O3) as a top coat on 7YSZ TBCs against CMAS/VA infiltration: Deposition and reaction mechanisms.* Journal of the European Ceramic Society, 2018. **38**(9): p. 3333-3346.
36. Chavez, J.J.G., et al., *Effects of Yttria Content on the CMAS Infiltration Resistance of Yttria Stabilized Thermal Barrier Coatings System.* Journal of Materials Science & Technology, 2019. **accepted**.

**Tables**

*Table 1: Summary of processing conditions and set up of the two coaters SMART and ESPRI*

| Topic | SMART Coater | ESPRI |
|---|---|---|
| **Rotation of parts with regard to ingot axis** | 90°; tilting possible but not used, 10 rpm | Parallel, no tilting, 12 rpm |
| **Distance between crucibles and middle of rotational axis** | 375 mm | 335 mm |
| **Change of evaporation between two crucibles** | Moving crucibles | Moving sample holder (sting) |
| **Sample fixture** | 3 positions, variable holder | Planetary drive (cylinders) or holder for flat samples |
| **Typical ingot feed rate** | 1.6 to 1.9 mm/min | 1.0 to 1.5 mm/min |
| **Deposition rate** | similar | |
| **Pre-heating time and temperature under vacuum** | 20 minutes into standby heated chamber; 1050°C | 10 minutes into hot heating chamber; 950 to 1000°C |
| **Substrate temperature range applied in the experiments** | 940 – 1050°C | 990 – 1030°C |
| **Gases in coating chamber** | $O_2$ + some Ar | $O_2$ |
| **Pressure in coating chamber and vacuum pumps** | $10^{-3}$ to $10^{-2}$ mbar, diffusion pump | $10^{-3}$ to $10^{-2}$ mbar, turbo pump |
| **Total power used for evaporation** | 100 to 120 kW | 65 to 75 kW |

*Table 2: Process conditions for all coating versions*

| **version** | **A** | **B** | **C** | **D** | **E** | **F** |
|---|---|---|---|---|---|---|
| **coater** | ESPRI | ESPRI | ESPRI | ESPRI | ESPRI | ESPRI |
| **Characte-risitic** | Bilayer | Bilayer | Bilayer | Single layer GZO | Single layer 7YSZ | Bilayer in two separate runs |
| **1st stage** | 7YSZ deposition | 7YSZ deposition | 7YSZ deposition | GZO deposition | 7YSZ deposition | 7YSZ deposition |
| **2nd stage** | slow transition from 7YSZ to GZO | fast switch from 7YSZ to GZO, sample motion (in parallel) | slow transition from 7YSZ to GZO, sample motion (in parallel) | | | removal from loading chamber, storage |
| **3rd stage** | GZO deposition | | | | | GZO deposition |
| **4th stage** | (delayed) sample motion | GZO deposition | GZO deposition | | | |

| **version** | **BS** | **ES** |
|---|---|---|
| **coater** | SMART | SMART |
| **Characte-risitic** | Bilayer | Single layer 7YSZ |
| **1st stage** | 7YSZ deposition | 7YSZ deposition |
| **2nd stage** | fast switch from 7YSZ to GZO, movement of crucibles | |
| **3rd stage** | | |

| | | |
|---|---|---|
| | (in parallel) | |
| **4th stage** | GZO deposition | |

Data of version D, E, and F are taken from [6]

Table 4: Thickness of the TBC layers. Numbers give the average values while the measured thicknesses varied by +/- 5 µm. Version E was taken from earlier studies [21] based on a larger number of samples originating from various deposition runs. Therefore, the variation in thickness was in this case +/-15 µm.

| **version** | **Thickness 1st layer (µm)** | **Thickness 2nd layer (µm)** |
|---|---|---|
| A | 35 | 145 (including 40 µm in first position) |
| B | 30 | 135 |
| BS | 82 | 80 |
| C | 25 | 145 |
| D<br>E<br>ES | 160<br>165<br>132 | |

**Figure captions**

Figure 1: EB-PVD coating equipment used in the current study. (a) Coater ESPRI at DLR, and (b) SMART coater at Rzeszow University of Technology.

Figure 2: Sketch of the arrangement of the two crucibles, electron beam gun, and part holder in the evaporation chambers. (a) ESPRI using moving sample holder, and (b) SMART coater using moving crucibles.

Figure 3: Lifetime in furnace cycle testing at 1100°C of the TBC versions investigated. Reference data of version E were taken from [21] and those of version D from [6].

Figure 4: Failure location of version A: (a) and (b) macroscopic pictures after 40 cycles, and (c) crack formation and propagation between 7YSZ and GZO after 40 cycles in SEM cross section.

Figure 5: Failure location of the bilayer TBCs having a longer life time and overview of microstructure in cross section. (a) Version B failure location mainly between 7YSZ and TGO after 2021 cycles, (b) version C failure location mainly between 7YSZ and TGO after 1023 cycles, and (c) version BS failure location between 7YSZ base layer and TGO after 1337 cycles, (d) version BS manufactured in a separate run applying a thin 7YSZ base layer and a thick GZO layer on a CMSX-4 substrate after 322 cycles.

Figure 6: High magnification SEM cross sections of the interface between 7 YSZ and GZO layer. (a) to (c) version A after 60 cycles, (d) version B after 40 cycles, (e) version C after 1023 cycles, (f) and (g) version BS after 1337 cycles, and (h) version BS after 1024 cycles. Circled areas indicate presence of gadolinium within the 7YSZ layer which was verified by EDS spot measurements.

Figure 7: Example of TGO formation in systems having a 7YSZ base layer; version BS after 1337 cycles

Figure 8: A modified version of BS manufactured in a separate run applying a thin 7YSZ base layer and a thick GZO layer on a CMSX-4 substrate after 322 cycles, indicating a straight growth of the bilayer columns.